Chemosphere 218 (2019) 299–307

Contents lists available at ScienceDirect

Chemosphere

journal homepage: www.elsevier.com/locate/chemosphere

Efficient degradation of diclofenac by $LaFeO_3$-Catalyzed peroxymonosulfate oxidation—kinetics and toxicity assessment

Yongfang Rao [a, *], Fuman Han [a], Qian Chen [a], Dan Wang [a], Dan Xue [a], Hua Wang [b], Shengyan Pu [c, **]

[a] Department of Environmental Science and Engineering, Xi' an Jiaotong University, Xi'an 710049, China
[b] Instrumental Analysis Center, Yancheng Teachers University, 2 South Xiwang Avenue, Yancheng 224007, China
[c] State Key Laboratory of Geohazard Prevention and Geoenvironment Protection (Chengdu University of Technology), 1#, Dongsanlu, Erxianqiao, Chengdu 610059, Sichuan, PR China

HIGHLIGHTS

- The catalytic activity of LFO is contingent on the calcination temperature of LFO.
- Diclofenac degradation rate depends on pH value, PMS and LFO dose.
- The marginal effect of LFO dosage is larger than that of PMS concentration.
- $H_2PO_4^-$ substantially inhibited DCF degradation.
- Toxicity elimination of DCF can be achieved by LFO/PMS process.

ARTICLE INFO

Article history:
Received 26 July 2018
Received in revised form
8 November 2018
Accepted 15 November 2018
Available online 16 November 2018

Handling Editor: Xiangru Zhang

Keywords:
Diclofenac
$LaFeO_3$
Peroxylmonosulfate
Degradation kinetic
Toxicity assessment

ABSTRACT

Diclofenac was frequently found in various waters, indicating conventional wastewater treatment methods ineffective in its removal. In this study, $LaFeO_3$ (LFO) was synthesized and its catalytic activity of LFO as the activator of different oxidants such as persulfate (PS), hydrogen peroxide and peroxylmonosulfate (PMS) was evaluated in terms of DCF degradation. The influence of calcination temperature was examined on the catalytic activity of LFO. The effects of various parameters including pH levels, PMS concentration, LFO dose and initial DCF concentration were investigated on DCF degradation rate. The marginal effects of PMS concentration and LFO dose were compared. Langmuir-Hinshelwood (LH) model was used to quantitatively describe DCF degradation reaction in LFO/PMS system. The two constants, k (Limiting reaction rate at maximum coverage) and K (Equilibrium adsorption constant), were determined on the basis of LH model. The performance of LFO/PMS process was also estimated in the presence of various inorganic anions. The potential toxicity of LFO and PMS were evaluated using phytoplankton and the toxicity evolution during DCF degradation was also investigated using luminescent bacteria. This contribution provides a basic study regarding the potential application of heterogeneous PMS activation by perovskite LFO for both DCF removal and toxicity elimination.

1. Introduction

In the past decade, pharmaceuticals, as emerging organic pollutants, have received ever-increasing concerns due to their ubiquity in water environment and documented harmful behavior (Corcoran et al., 2010; Gavrilescu et al., 2015). In 2013, pharmaceuticals were legally deemed as a potential hazard for the aquatic environment in an amendment of the EU water framework directive. This directive contains a watch list of compounds which demand recording, tracking and evaluating of their environmental risks to support their classification. Diclofenac (DCF) was included in the first watch list (EU, 2013).

Advanced oxidation processes (AOPs) are considered as desirable technologies for the degradation and mineralization of persistent organic pollutants (POPs) through radical oxidation. DCF

* Corresponding author.
** Corresponding author.
E-mail addresses: yfrao@mail.xjtu.edu.cn (Y. Rao), pushengyan@gmail.com (S. Pu).

https://doi.org/10.1016/j.chemosphere.2018.11.105
0045-6535/

has been subjected to many studies on its treatability by various AOPs, including photocatalysis (Chen et al., 2018), ozonation (Sein et al., 2008), sonication (Al-Hamadani et al., 2018) and Fenton oxidation (Zhou et al., 2018). In the past decade, there is an increasing interest in sulfate radical anion based oxidation for POPs removal. Sulfate radical with a redox potential of 2.5–3.1 V exhibited relatively high selectivity towards aromatic/unsaturated chemical structures (Neta et al., 1988) with a much longer half-life than hydroxyl radical (Janzen et al., 1992; Olmez-Hanci and Arslan-Alaton, 2013). The generation of sulfate radical can be achieved via the activation of peroxydisulfate (PDS) or peroxymonosulfate (PMS) by thermal (Yang et al., 2010), UV light (Lau et al., 2007; Guan et al., 2011), ultrasound (Hao et al., 2014) and transition metal ions (Rao et al., 2014). Among these methods, activation of PMS or PDS by transition metal ions is considered more cost-effective since the other processes demand continuous energy input. Although Cobalt (II) was an effective activator for PMS to generate sulfate radical among the transition metal ions, it is not the optimal choice due to its potential adverse health effects. Even for Co_3O_4 or supported cobalt oxide, concerns about leaching of cobalt from the solid phase still rein in their practical application in water treatment. On the other side, iron, the second most abundant element in the earth, is not considered to pose a potential risk on human health and ecological system. It has been reported both Fe_2O_3 and Fe_3O_4 can activate PMS to generate sulfate radicals in previous studies (Ji et al., 2013; Tan et al., 2014; Jaafarzadeh et al., 2017). Su et al. (2017) observed the perovskite oxide could promote an easier valence-state change of the B-site cation (cobalt ions) to accelerate a redox process. In recent years, using perovskite-type oxides (PTOs) to activate PMS has attracted increasing attention (Pang et al., 2016; Ben Hammouda et al., 2017; Solis et al., 2017; Su et al., 2017; Duan et al., 2018; Miao et al., 2018). Cobalt-based PTOs exhibited much higher activity toward PMS than Co_3O_4 did. However, the investigation on the use of Fe-based PTOs as an activator of PMS is limited. In our previous study, LFO also showed much better performance than Fe_2O_3 did in term of activating PMS for DCF degradation. The Fe (III) in LFO perovskite oxide can be reduced more easily than Fe (III) in Fe_2O_3. The generation of sulfate radicals which made a major contribution to DCF degradation is ascribed to the formation of inner-sphere complexation between Fe (III) and HSO_5^- and Fe (III) –Fe (II)–Fe (III) redox cycle (Rao et al., 2018).

The burgeoning applications of nanomaterials have invited environment, health and safety concerns in recent years. Servin et al. (2013) verified the accumulation of TiO_2 nanoparticles in cucumber. CuO nanoparticles were reported to exert a toxic effect on Prokaryotic alga *Microcystis aeruginosa* and the presence of fulvic acid increased its toxicity (Wang et al., 2011). Furthermore, 2.5 mM PMS was observed to inhibit the growth of freshwater microalgae *Pseudokirchneriella subcapitata* significantly (Olmez-Hanci et al., 2014). However, the toxicity of PMS at low concentration to phytoplankton remains unknown. It was reported that the intermediates generated during the degradation of pharmaceuticals by some AOPs might be more toxic than parent compounds. In our previous study, the EC_{50-96h} (Half maximal effective concentration for 96 h) of both solutions after 30-min and 60-min sonication is lower than that of initial carbamazepine solution (Rao et al., 2016). Chen et al. (2016) reported that the toxicity of intermediates in both ozonation and catalytic ozonation processes had increased, in comparison with that of DCF in the first 15 min of DCF degradation. Thus, the ecotoxicity evolution of the treated wastewater containing DCF should also be properly evaluated.

In this study, we focused on the optimization of LFO/PMS process conditions through examining the influence of various parameters such as pH value, LFO dosage, PMS concentration and DCF concentration on DCF degradation. The effect of calcination temperature on the activity of as-prepared catalyst $LaFeO_3$ was evaluated. The potential toxicity of LFO and PMS was evaluated towards phytoplankton. The evolution of the acute toxicity was also examined during DCF degradation.

2. Materials and methods

2.1. Chemicals

Iron nitrate nonahydrate ($Fe(NO_3)_3 \cdot 9H_2O$), citric acid monohydrate ($C_6H_8O_7 \cdot H_2O$), 2, 6-dichloroaniline and sodium tetraborate were purchased from Sinopharm Chemical Reagent Co., Ltd, China. Diclofenac (2-[2,6-dichlorophenyl]-amino]-benzene acetic acid sodium salt), Oxone and Lanthanum nitrate hexahydrate ($La(NO_3)_3 \cdot 6H_2O$) were obtained from Sigma-Aldrich. All solvents were HPLC grade. All chemicals are in analytic purity and used without purification. All aqueous solutions were prepared in distilled and deionized water (DDW) with a resistivity of 18.0 MΩ from a Millipore Waters Milli-Q water purification system.

2.2. Catalyst synthesis and characterization

The synthesis procedure of perovskite LFO has been described in our previous study (Rao et al., 2018).

X-ray powder diffraction (XRD) with Cu Kα radiation at a scan rate of 0.05°/s (λ = 1.5406 Å, 40 kV, 40 mA, PANalytical X' Pert PRO X-ray diffractometer) was used to determine the crystal structure of as-prepared samples. The N_2 adsorption/desorption isotherms at 77 K employing an ASAP 2020 automatic analyzer (Micromeritics Instrument Corp., Norcross, GA, USA) were analyzed to determine the Brunauer–Emmett–Teller (BET) surface area and pore structure of the as-prepared catalysts. The mean hydrodynamic diameter of as-prepared catalysts was measured by a Brookhaven Zetasizer Nano ZS90Plus.

2.3. Batch reaction

LFO-activated PMS for DCF degradation was carried out in a magnetically stirred batch reactor. Specific aliquots of 0.2 mM DCF stock solution with DDW as solvent were pipetted into the reactors to achieve a prearranged initial concentration. Different dosage of as-prepared LFO was added into 100 mL DCF solution, followed by sonication for 5 min. Appropriate amount of PMS stock solution was added into the reactor to initiate the catalytic reaction. At prearranged time intervals, 1 mL of the reaction solution was withdrawn and filtered through a 0.2 μm Millipore PTFE membrane into a vial with Sodium thiosulfate as a quenching agent. The solution was then analyzed by High Performance Liquid Chromatography (HPLC) to quantify the remaining DCF. All experiments were conducted in duplicate and the error is less than 5.0%.

2.4. Toxicity test

Chlorella vulgaris (*C. vulgaris*) was purchased from the Institute of hydrobiology, Chinese Academy of Sciences (China) to assess the toxicity of LFO and PMS towards phytoplankton. The algae cells were cultured in f/2 medium. Predetermined dosage of LFO powder was added to the algal medium for a test group. Stock solutions of PMS and SO_4^{2-} were dispensed to the algal medium to reach the desired concentration for other test groups. Pure f/2 medium was used as the control group. Exponentially growing *C. vulgaris* in f/2 medium with predetermined density were transferred to a flask with various test solutions and control solution to obtain a rough density of $0.85–1.05 \times 10^7$ cells mL^{-1}. Following their inoculation with *C. vulgaris*, the test flasks were sealed with gauzes and

cultured in artificial climate incubators (2000 lux, 12 h light/12 h dark and 298 ± 1 K). Growth of the cultures was calculated every 2 days by measuring the optical density of the cell suspension at 680 nm using a spectrophotometer (UV-2800, UNICO, Shanghai, China) (Baran et al., 2006).

The acute toxicity of DCF and its intermediates generated during the catalytic oxidation of DCF was evaluated by measuring the effect of the samples toward the bioluminescence of *Photobacterium phosphoreum* T3 using Modulus™ single-tube luminometer (TurnerBioSystems, USA). The *Photobacterium phosphoreum* bacteria were provided by China General Microbiological Culture Collection Center (CGMCC). The bioluminescence of *Photobacterium phosphoreum* T3 was measured after incubation in solution samples or DDW for 15 min and the relative luminescence (%) was calculated as follows:

$$\text{Relative luminescence} = \frac{\text{luminescence of T3 in solution samples}}{\text{luminescence of T3 in DDW}}$$

3. Results and discussion

3.1. XRD characterizations and pore structure of as-prepared LFO

Fig. S1 shows the XRD patterns of as-prepared LFO calcined at different temperature. The characteristic diffraction peaks located at 22.6°, 32.2°, 39.7°, 46.2°, 57.5°, 67.5° indicate the successful synthesis of phase-pure LFO. The molar ratio of La and Fe in LFO was determined to be 1:1.04 based on the ICP analysis of La and Fe content after the acid-digestion of LFO, further confirming the synthesized samples are LFO. As also illustrated in Fig. S1, the increasing intensity of those diffraction peaks of as-prepared samples can be observed at the elevated calcination temperature. The mean crystallite size of as-synthesized samples calcined at different temperature is about 18.4 nm, 20.6 nm, 22.8 nm and 26.5 nm, respectively, as determined by Scherrer Equation based on the strongest 121 diffraction peak.

The N_2 adsorption/desorption isotherms of as-prepared samples were used to determine the BET specific surface area, pore-size distribution, and pore volume (See Fig. S2). The shape of the physisorption isotherms for LFO-500, LFO-600 and LFO-700 is in line with type IV showing type H3 hysteresis loops in the P/P_0 range of 0.7–1.0, 0.75–1.0 and 0.4–0.98, respectively. The shape of the physisorption isotherm of LFO-900 agrees with type IV exhibiting type H4 hysteresis loop in the P/P_0 range of 0.2–1.0. These are the typical characteristics of mesopores, according to IUPAC classification. The pore diameter, pore volume and surface area of LFO catalysts calcined at different temperature are presented in Table S1.

3.2. DCF degradation by different oxidants catalyzed by LFO-500

In order to evaluate the activity of LFO to catalyze different oxidants, LFO was used to activate H_2O_2, $S_2O_8^{2-}$ and PMS for DCF degradation. As shown in Fig. 1, the rapid degradation of DCF was only observed in LFO/PMS system. It was reported that the O–O bond length in HSO_5^-, H_2O_2 and $S_2O_8^{2-}$ is 1.460, 1.453 and 1.497 Å, respectively (Flanagan et al., 1984). The energy of O–O bond in PS was estimated to be 140 kJ mol^{-1} (Kolthoff and Miller, 1951) while that in H_2O_2 was reported to be 210.3 kJ mol^{-1} (Gray, 1959). The bond energy of O–O in PMS is supposed to be between 140 and 210.3 kJ mol^{-1}. Although the bond energy of O–O in PMS may be greater than that in PS, PMS has an asymmetric structure with SO_3 replaced by H on one side. The asymmetric structure of HSO_5^- may favor it replacing surface –OH of LFO to bond with the Fe (III) of LFO.

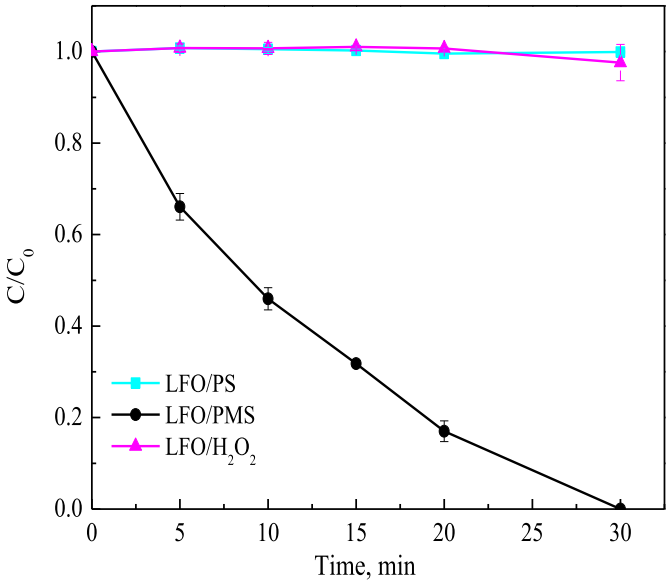

Fig. 1. DCF degradation by different oxidants catalyzed by LFO-500. (Notes: $[DCF]_0 = 0.025$ mM, $[LFO] = 0.1$ g L^{-1}, $[oxidant]_0 = 0.5$ mM, pH 6.0–7.0 bufferred with tetraborate).

3.3. Effects of calcination temperature on the activity of LFO

Fig. 2 describes DCF degradation by PMS activated by LFO calcined at different temperature. The catalytic activity of LFO decreased with the enhancement of calcination temperature. As shown in Table S1, the BET surface area and pore volume of LFO decline with the increase of calcination temperature, suggesting the higher calcination temperature, the less active sites available on LFO surface. Furthermore, the hydrodynamic diameter of LFO-500, LFO-600, LFO-700 and LFO-900 was measured to be 305, 757, 1215 and 12346 nm, respectively. LFO-900 particles are much larger than other particles, leading to less active sites exposed. The reduction of

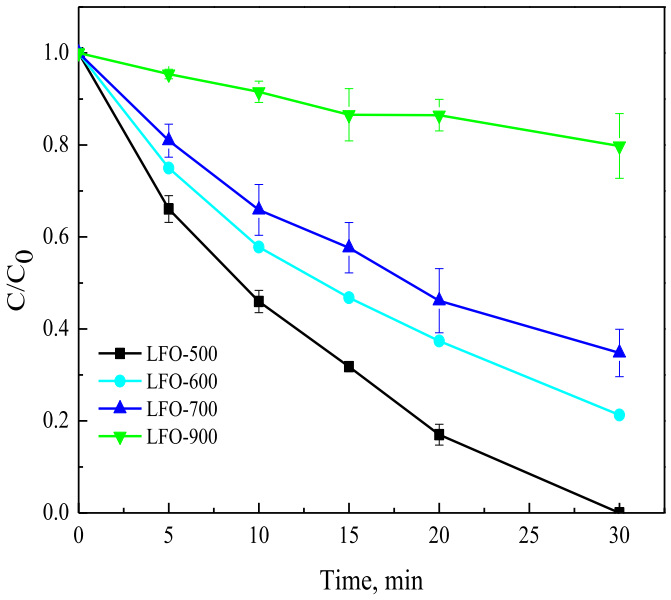

Fig. 2. Effects of calcination temperature on the activity of LFO. (Notes: $[DCF]_0 = 0.025$ mM, $[LFO] = 0.1$ g L^{-1}, $[PMS]_0 = 0.5$ mM, pH 6.0–7.0 bufferred with tetraborate).

active sites is unfavorable for the adsorption of HSO_5^- and DCF on LFO surface, leading to the drop-off of LFO activity. According to our previous study (Rao et al., 2018), the active metal site of LFO is Fe (III) and hydroxyl group on the surface of LFO is important for the interaction between Fe (III) and HSO_5^-. Therefore, the surface chemical states of LFO calcined at different temperature were compared (See Fig. S3). As shown in Fig. S3a, the two peaks of Fe 2p of these four samples are quite similar, indicating calcination temperature play an insignificant role in the oxidation state of Fe. The asymmetric shape of O 1s peak can be deconvolved into two separate peaks at around 528.7 and 530.0 eV (Fig. S3b), which are attributed to the lattice oxygen (O_L) and surface hydroxyl groups (O_H). As the calcination temperature increases from 500 to 900 °C, the area ratio of O_H on the surface of LFO decreased from 58.6% to 28.2%, further justifying the decreased activities of LFO at the elevated calcination temperature.

As a result, LFO-500 was selected as the sole catalyst in the following study.

3.4. Influence of pH level

It is well-known that the performance of sulfate radical-based AOPs is strongly dependent on the solution pH value. DCF degradation was examined at different pH levels varying from 5.1 to 9.0 in this study. As shown in Fig. 3a, pH levels exerted significant influence on the performance of LFO/PMS process; the fastest decay rate of DCF was observed at pH 7.0. DCF degradation rate declined under acidic and alkaline conditions. The pKa_1 of H_2SO_5 is below 0 (Negri et al., 1998) and the pKa_2 is 9.4 (Maruthamuthu and Neta, 1977), implying the only existence for PMS species is HSO_5^- in reaction solution at pH ≤ 7 and a small portion of SO_5^{2-} is present at pH 9.0. It was reported the uncatalyzed decomposition rate of PMS was the fastest at pH of 9.3 (Ball and Edwards, 1956; Goodman and Robson, 1963). At pH 9.0, the uncatalyzed decomposition contributed considerably to the rapid decomposition of PMS (See Fig. 3b), leading to less HSO_5^- ions available to be activated by LFO. On the other side, the pH_{pzc} of LFO was determined to be roughly 9.3 (Rao et al., 2018). The enhancement of pH value close to its pH_{pzc} reduced the amount of positive surface charge, which may decrease the electrostatic attraction between LFO and PMS species. DCF degradation was inhibited under acidic conditions, which was also observed in a previous report (Zhang et al., 2013). It was speculated that the formation of hydrogen bond between hydrogen ion and the O—O group of HSO_5^- would be favorable under acidic condition, neutralizing the negative charge carried by part of HSO_5^- ions and hampering their interaction with the positively-charged LFO surface (Zhang et al., 2013). As illustrated in Fig. 3b, PMS decomposition was inhibited under acidic conditions.

3.5. Effects of PMS concentration

PMS concentration is a critical parameter since PMS is the sole source of sulfate radicals in LFO/PMS process. The influence of PMS dosages on DCF decay was examined with LFO dosage fixed at 0.1 g L^{-1} and pH at 7.0 ± 0.5. DCF degradation was found to fit pseudo first-order kinetics well. As demonstrated in Fig. 4a, the DCF degradation rate constant ramps up linearly with the enhancement of PMS concentration from 0.1 to 0.5 mM with R^2 of 0.98. However, the further enhancement of PMS concentration decelerated DCF degradation. The amount of active sites on the surface of LFO particles is supposed to be constant since LFO dosage was fixed. On the other side, the overdosed PMS (See Fig. 4b) which could not be activated by LFO can consume sulfate radicals, leading to the decline of DCF degradation rate. When 0.6 and 0.7 mM PMS was dosed, the residual PMS concentration is 0.36 mM and 0.455 mM after 30 min in the reaction system, respectively.

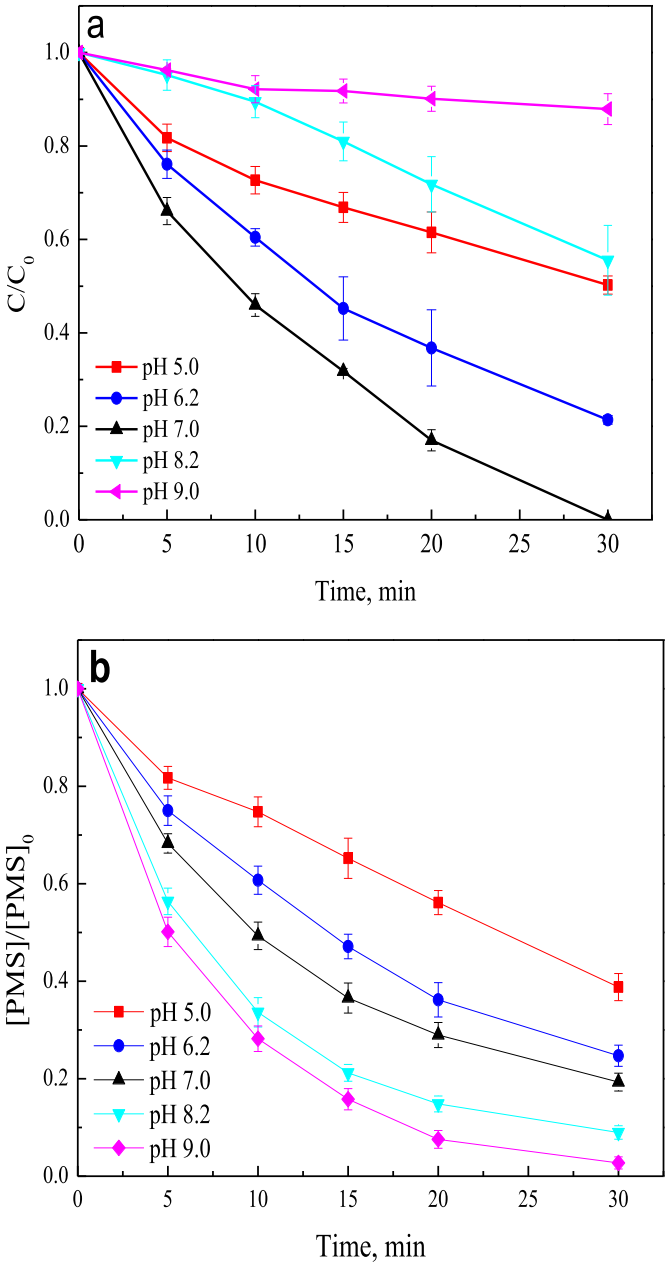

Fig. 3. (a) Effects of pH on DCF degradation by LFO/PMS process; (b) Effects of pH on PMS degradation during catalytic oxidation of DCF (Notes: $[DCF]_0 = 0.025$ mM, LFO dosage = 0.1 g L^{-1}, $[PMS]_0 = 0.5$ mM, tetraborate adjusted pH).

3.6. Effects of LFO dosage

Proper dosage of LFO, served as an activator of PMS, is also an important parameter for the LFO/PMS process. In this study, DCF degradation rate at different LFO dosages (ranging from 0.1 to 0.8 g L^{-1}) were examined with the initial PMS concentration fixed at 0.5 mM and pH at 7.0 ± 0.5. DCF degradation at different LFO dosage also fit pseudo first-order kinetics well ($R^2 > 0.96$). The rising LFO dosage renders more active sites available for the activation of PMS, which was indirectly evidenced by the increase of PMS decomposition rate (See Fig. 5b), resulting in the generation of more sulfate radicals. Thus, DCF degradation rate ramped up with

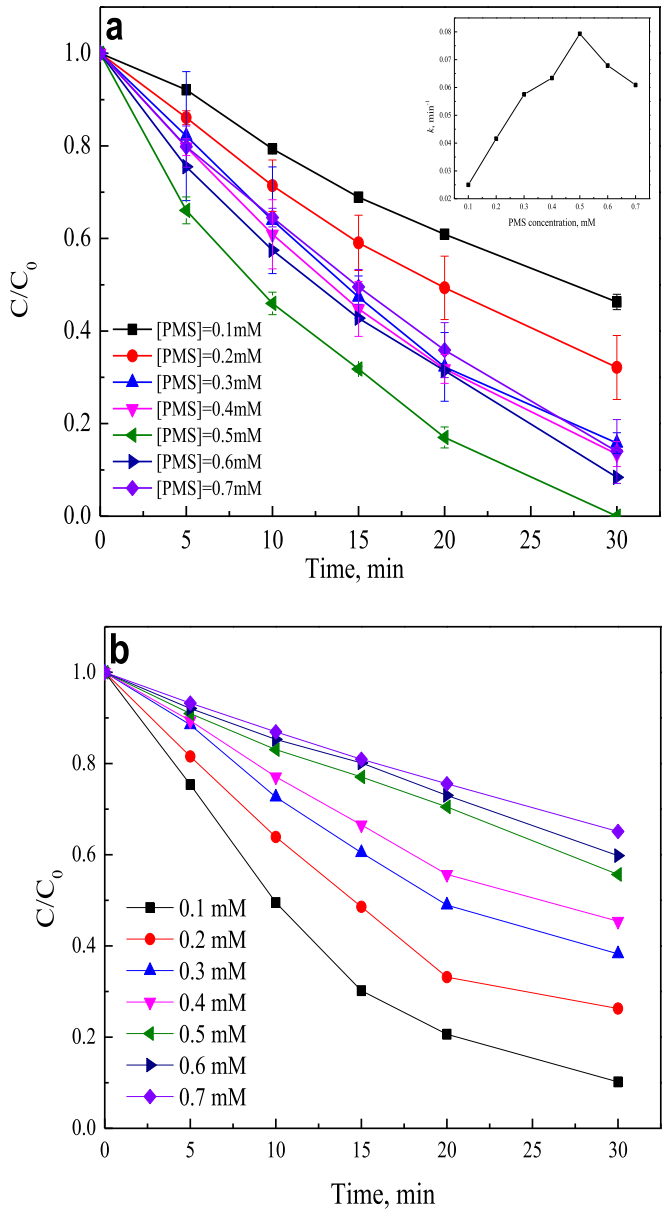

Fig. 4. (a) Effects of PMS concentration on DCF degradation; (b) PMS decomposition at different initial PMS concentration (Notes: $[DCF]_0 = 0.025$ mM, $[LFO] = 0.1\ g\ L^{-1}$, pH 6.0–7.0 bufferred with tetraborate).

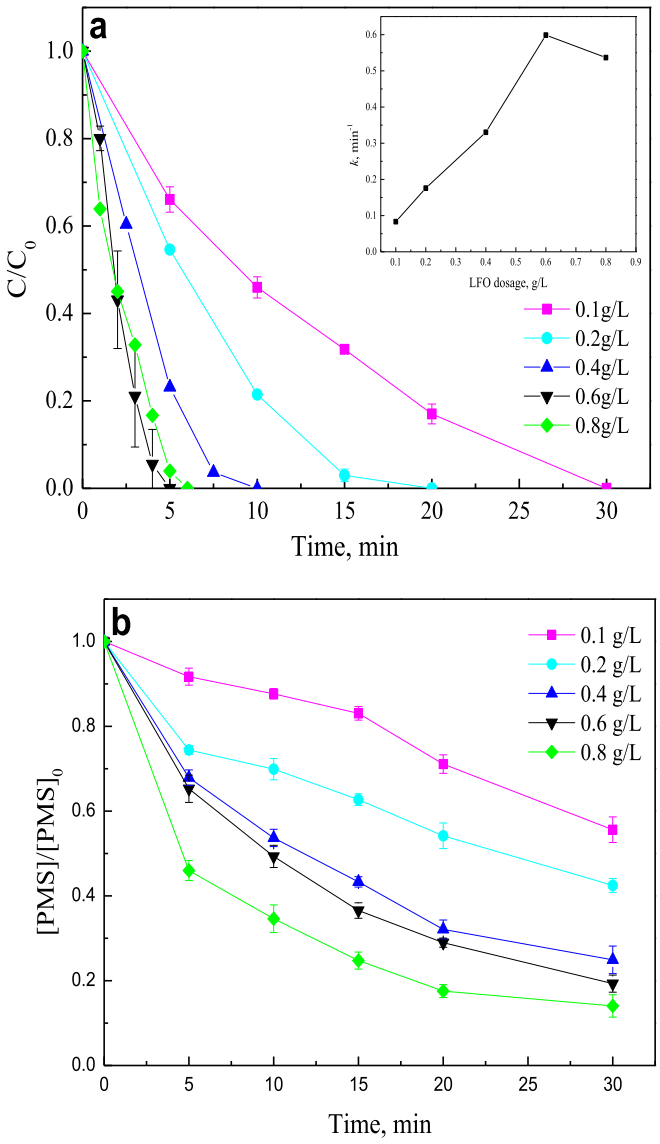

Fig. 5. (a) Effects of LFO dose on DCF degradation; (b) PMS decomposition at different LFO dose (Notes: $[DCF]_0 = 0.025$ mM, $[PMS]_0 = 0.5$ mM, pH 6.0–7.0 bufferred with tetraborate).

the increase of LFO dosage from 0.1 to 0.6 g L^{-1} (See Fig. 5a). Fig. 5a shows optimal LFO dosage at 0.6 g L^{-1}. As also indicated in the inset of Fig. 5a, linear relationship was found between the reaction rate constant and the LFO dosage below its optimal value with R^2 around 0.98. Although the consumption of PMS at 0.8 g L^{-1} LFO dosage was more than that at 0.6 g L^{-1} dosage (See Fig. 5b), the decrease of DCF degradation reaction rate constant was observed. This can be attributed to diffusion limitation during heterogeneous reactions (Zhang et al., 2013). The HSO_5^- ions may diffuse faster toward the Fe (III) sites of LFO than DCF due to its smaller size and the hydrophlicity of LFO, on the surface of which there are many hydroxyl groups (Rao et al., 2018). Thus, side-reactions such as reactions between $SO_4^{\bullet-}$ and HSO_5^-, and $SO_4^{\bullet-}$ combining with each other to form $S_2O_8^{2-}$, might consume sulfate radicals before DCF arriving at LFO surface, leading to the ineffective consumption of PMS.

In order to compare the marginal effect of the two parameters (PMS concentration and LFO dosage), the LFO dosage and PMS concentration were normalized. As shown in Fig. S4, both curves can be divided into two sections, viz. the ratio of [dosage]/[optimum dosage] smaller and larger than unity. It can also be observed that [LFO] dosage exhibited more significant influence on the performance of LFO/PMS process than PMS concentration did. This implies the selection of LFO dosage is more important than that of PMS concentration in the design of this process.

3.7. Effect of the initial concentration of DCF

DCF degradation was tested with varied initial concentration as illustrated in Fig. 6a. The observed DCF degradation reaction rate constant declined with the increase of initial concentration under the same conditions.

The Langmuir-Hinshelwood (LH) kinetics can be employed to quantitatively describe the reactions at solid-liquid interface in

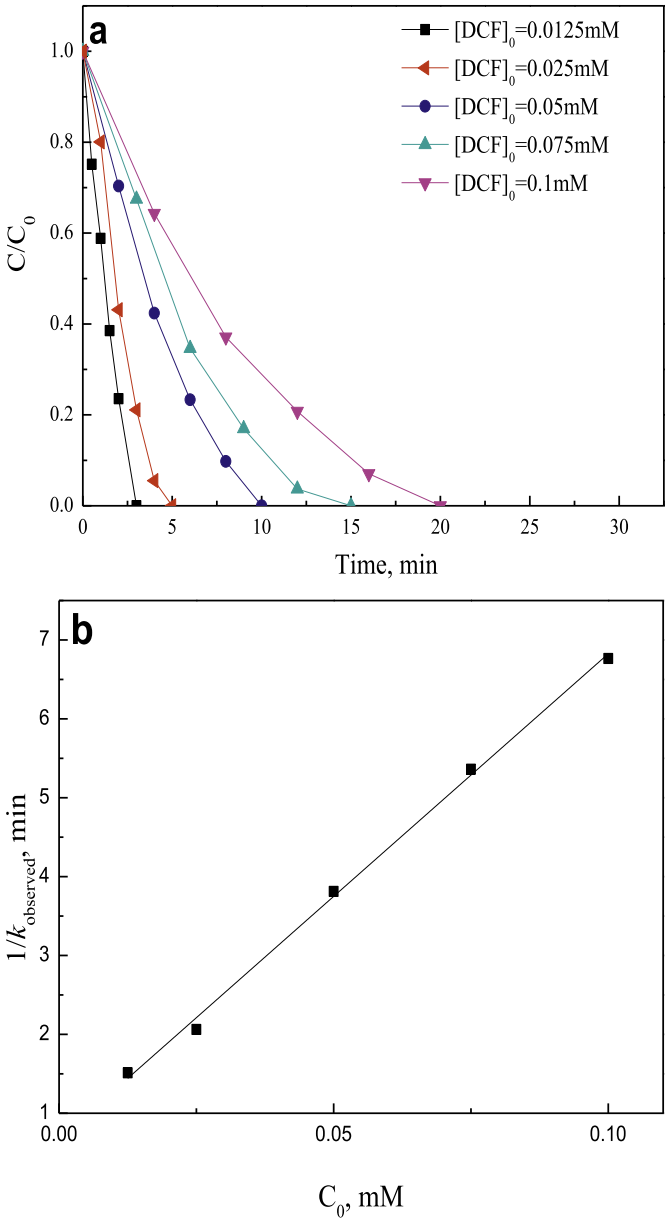

Fig. 6. (a) Effects of DCF initial concentration; (b) $1/k_{observed}$ vs C_0 (Notes: [LFO] = 0.6 g L^{-1}, $[PMS]_0$ = 0.5 mM, pH 6.0–7.0 bufferred with tetraborate).

heterogeneous catalysis systems based on the assumption that the homogeneous reaction is inconsequential and surface reaction of adsorbed species is the limiting step. The effects of methanol and ethanol on DCF degradation were insignificant in this system (Rao et al., 2018), indicating that the oxidative degradation of DCF mainly took place on the LFO surface. Therefore, it is reasonable that LH model is used to delineate DCF degradation on LFO surface. The initial rate, r_0, can be expressed as:

$$r_0 = -\frac{dC_0}{dt} = \frac{kKC_0}{1+KC_0} \quad (1)$$

where C_0 is the initial concentration of DCF, K is the equilibrium adsorption constant of DCF on LFO surface (mM^{-1}) and k represents the limiting reaction rate at maximum coverage in this system (mM min^{-1}).

In the case of pseudo first-order kinetics, the incorporation of $-dC_0/dt = k_{observed}C_o$ into Eq. (1) gives:

$$k_{observed} = \frac{kK}{1+KC_0} \quad (2)$$

Eq. (3) can be obtained by the linearization of Eq. (2):

$$\frac{1}{k_{observed}} = \frac{1}{k}C_0 + \frac{1}{kK} \quad (3)$$

Then, $1/k_{observed}$ vs C_0 was plotted in Fig. 6b. DCF degradation at various initial concentrations fits the LH model well with R^2 of 0.998, implying the assumption of surface reaction is reasonable. The two constants, k and K, were decided to be 0.0163 mM min^{-1} and 91.4 mM^{-1} from the slope and intercept, respectively. Thus, DCF degradation rate can be predicted when the initial concentration is known under the same conditions.

3.8. Effects of inorganic anions

Inorganic anions exist in various waters. The presence of some inorganic anions was found to affect the degradation of organic pollutants by sulfate radicals-based AOPs in previous studies which observed contradictory results (Chan and Chu, 2009; Wang and Chu, 2011; Rao et al., 2014; Lin et al., 2017). The way chloride ions influence the degradation of organic compounds by AOPs was reported to depend on their molecular structure (Yang et al., 2014). Thus, it is necessary to evaluate the effects of various inorganic anions on DCF decomposition in LFO/PMS system for a practical application. Fig. S5 shows the effects exerted by four inorganic anions, including Cl^-, NO_3^-, SO_4^{2-} and $H_2PO_4^-$ on DCF degradation. Chloride, nitrate and sulfate ions exerted insignificant influence on DCF degradation while DCF degradation was remarkably inhibited in the presence of $H_2PO_4^-$. At pH 7.0, $H_2PO_4^-$ and HPO_4^{2-} are dominating species in the reaction solution. LFO surface was positively charged at pH 7.0 since the pH_{pzc} of LFO was around 9.3. The binding affinity of HPO_4^{2-} toward Fe (III) on the LFO surface is stronger than that of HSO_5^-, leading to the formation of inner sphere complexes between HSO_5^- and Fe (III) being inhibited. Chloride ion can be oxidized by hydroxyl and sulfate radicals to form $Cl^•$ and $Cl_2^{•-}$ through a series of chain reactions. With the presence of the relatively high concentration chloride, these chain reactions could result in a significant consumption of $SO_4^{•-}$ in aqueous phase due to their high reaction rate constant (Neta et al., 1988; Anipsitakis et al., 2006). In this work, the concentration of chloride ions is 10 mM, which is much higher than that of DCF. However, LFO-activated PMS is a surface reaction. The HSO_5^- ions forming inner sphere complex with Fe (III) of LFO may repel the approach of chloride ions due to the electrostatic repulsion. Thus, chloride ions fail to scavenge $SO_4^{•-}$ significantly. Furthermore, the molecular structure of DCF contains two benzene rings which are linked by an imino group. One benzene ring is attached by two chlorines and the other one has a side chain of acetic acid group. $Cl^•$ and $Cl_2^{•-}$ are less reactive and more selective than hydroxyl and sulfate radicals. They can attack the electron-rich compound or group efficiently. The benzene ring with two chlorine atom substituents is electron-deficient, which is not conducive to the attack of $Cl^•$ and $Cl_2^{•-}$. For the case of another benzene ring, the group of acetic acid is electron-withdrawing. Although the imino group is electron-donating, the imino group may fail to donate electron to the benzene ring with acetic acid due to the strong electron-withdrawing capability of two chlorines. As a result, the benzene ring with acetic acid group is also not susceptible to the attack of $Cl^•$ and $Cl_2^{•-}$.

3.9. Toxicity assays

3.9.1. Potential toxicity of PMS and LFO towards C. vulgaris

The effect of oxone and LFO on the growth of algae *C. vulgaris* was first examined to assess their potential toxicity in aquatic environment. Fig. 7a indicates the growth of *C. vulgaris* was completely inhibited in the presence of oxone at high concentration (0.2 mM). The addition of oxone with concentration at 0.1 mM inhibited the growth of *C. vulgaris* during the initial 6 days while significantly accelerating the growth of *C. vulgaris* after 6 days (See Fig. S6). The inhibiting effects of oxone at high concentration may be attributed to the enhanced redox potential (422 mV) of the medium compared to that (236 mV) of the pure f/2 medium. In a separate experiment, a flask of f/2 medium with the presence of 0.1 mM Oxone solution was also placed in artificial climate incubators for 8 days. The redox potential declined from 422 to 230 mV due to the decomposition of around 67% of 0.1 mM Oxone after 6 days incubation. The results rationalized the increased growth of *C. vulgaris* with the presence of 0.1 mM Oxone after 6 days. It was found that the 0.1 μM oxone appreciably promoted *C. vulgaris* growth during the whole 14-day incubation. As also demonstrated in Fig. 7a, the presence of 0.2 μM SO_4^{2-}, which equals to the amount of SO_4^{2-} contained in 0.1 μM oxone, boosted the growth rate of *C. vulgaris* like 0.1 μM oxone did, indicating that SO_4^{2-} ions account for the promoting effect of oxone. It was reported that NO_3^- could act as an electron acceptor (Delatorre et al., 1991) and accelerate the light-induced charge transfer from O_2-evolving system to the primary electron acceptor of photosystem 2 in *C. vulgaris* cells (Osman and El-Naggar, 1999). It is reasonable to assume SO_4^{2-} played similar roles as NO_3^- did during *C. vulgaris* growth. Fig. 7a also shows LFO exerted insignificant influence on the growth of *C. vulgaris*, suggesting that LFO is an environmentally benign nanomaterial.

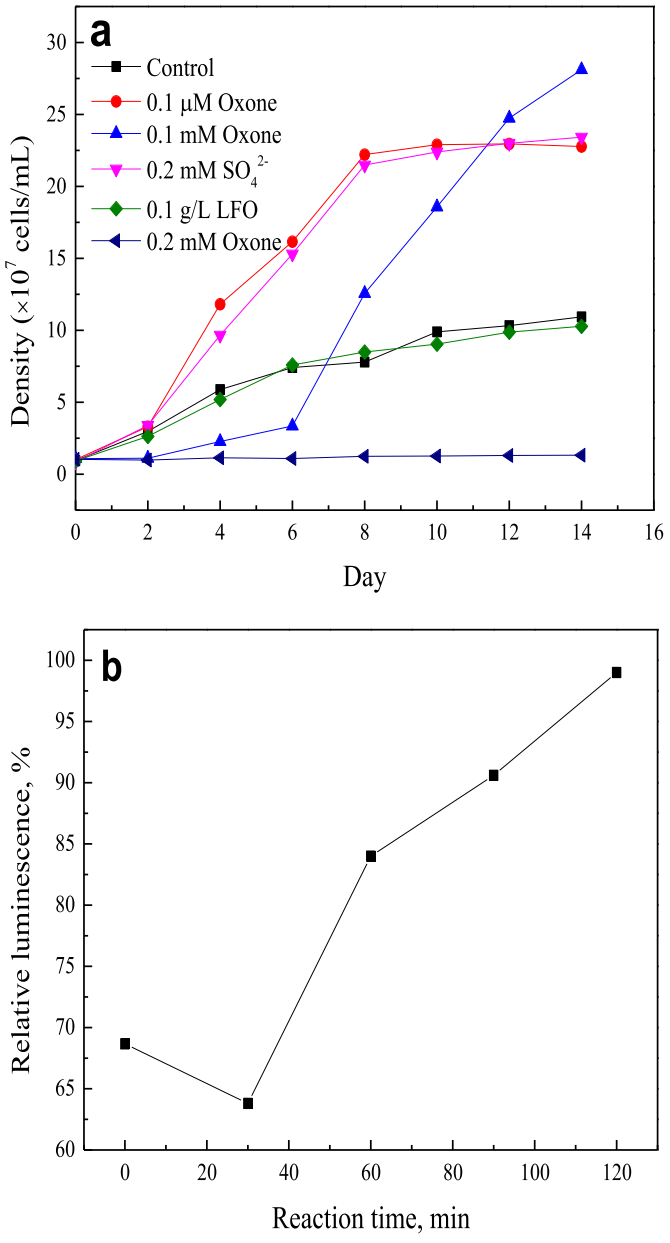

Fig. 7. (a) Effects of PMS, SO_4^{2-} and LFO on the growth of *C. vulgaris*; (b) Toxicity evolution during DCF degradation using *Photobacterium phosphoreum* T3 (Notes: $[DCF]_0 = 0.05$ mM, LFO dosage = 0.2 g L^{-1}, $[PMS]_0 = 0.3$ mM, tetraborate adjusted pH 6.0–7.0).

3.9.2. Toxicity evolution during DCF degradation process

The effects of DCF and the degradation intermediates on the *Photobacterium phosphoreum* T3 were examined to illuminate the toxicity evolution during DCF degradation by LFO/PMS process. In this study, PMS was observed to inhibit the bioluminescence of *Photobacterium phosphoreum* T3 significantly at high concentration with EC_{50} of 0.12 mM, rendering it impossible to evaluate the toxicity variation of DCF intermediates over time directly. It was also observed that sulfite and sulfate ions were innocuous to *Photobacterium phosphoreum* T3. Therefore, the toxicity interference caused by PMS can be eliminated by using a stoichiometric amount of Na_2SO_3 to reduce the residual PMS ions to sulfate ions.

The relative bioluminescence of *Photobacterium phosphoreum* T3 incubated in DCF and reaction solutions, which were taken at different time intervals during DCF degradation was illustrated in Fig. 7b. The relative bioluminescence of T3 decreased from 68.7% at 0 min to 63.8% at 30 min. This may be due to the accumulation of the intermediates which are more toxic than DCF. The EC50 of 2, 6-dichloroaniline, one of the intermediates generated during DCF degradation process, was measured to be 0.033 mM while EC50 of DCF was 0.086 mM, indicating that 2, 6-dichloroaniline is more toxic than DCF in term of bioluminescence inhibition of *Photobacterium phosphoreum* T3. The inhibiting effects of the degradation intermediates decreased gradually after 30 min of oxidation reaction and the bioluminescence of *Photobacterium phosphoreum* T3 in the reaction solution rose to the level similar to that in control group after 120 min. This is because the toxic intermediates suffered ring opening to generate nontoxic low molecular weight organic acid such as formic acid, acetic acid and lactic acid, and further mineralization (Rao et al., 2018).

4. Conclusions

In this study, LFO was synthesized. LFO was found to be an effective activator of PMS for the elimination of DCF in aqueous phase. DCF degradation data fit pseudo first-order kinetics well ($R^2 > 0.96$). The catalytic activity of LFO depends on the calcination temperature of LFO. Experimental results also show that the performance of LFO/PMS was influenced by pH levels, LFO dose and PMS concentration. The optimal pH is around 7.0. The optimal concentration of PMS is 0.5 mM with the LFO dosage fixed at 0.1 g L^{-1} and pH at 7.0. The best performance of LFO/PMS was found at the LFO dosage of 0.6 g L^{-1} with the PMS concentration fixed at 0.5 mM and pH 7.0. The linear relationship can be established between the observed rate constant and LFO dose below the optimal

value. LFO dosage exerted more important influence than PMS concentration did on DCF degradation by LFO/PMS process. Nitrate, sulfate and chloride ions showed no significant effect on DCF decay rate while $H_2PO_4^-$ considerably inhibited DCF degradation by LFO/PMS process. DCF degradation fits the LH model well in LFO/PMS system. The two constants, k (Limiting reaction rate at maximum coverage) and K (Equilibrium adsorption constant), were determined to be 0.0163 mM min^{-1} and 91.4 mM^{-1}. The LFO particles showed no toxic effect on the growth of *C. vulgaris*. The acute toxicity of DCF towards *Photobacterium phosphoreum* T3 can be completely eradicated after 120 min of reaction. The results indicate that LFO-activated PMS is an effective and environmentally-friendly technique for the removal and toxicity elimination of recalcitrant pharmaceuticals.

Acknowledgements

This work was financially supported by National Science Foundation of China (No.41877480), Shaanxi Natural Science Foundation, China (No. 2017JM5074) and Open project of Jiangsu Key Laboratory for Bioresources of Saline Solis. The authors are also grateful to all anonymous reviewers who contribute to improving this work.

Appendix A. Supplementary data

Supplementary data to this article can be found online at https://doi.org/10.1016/j.chemosphere.2018.11.105.

References

Al-Hamadani, Y.A.J., Lee, G., Kim, S., Park, C.M., Jang, M., Her, N., Han, J., Kim, D.H., Yoon, Y., 2018. Sonocatalytic degradation of carbamazepine and diclofenac in the presence of graphene oxides in aqueous solution. Chemosphere 205, 719–727.

Anipsitakis, G.P., Dionysiou, D.D., Gonzalez, M.A., 2006. Cobalt-mediated activation of peroxymonosulfate and sulfate radical attack on phenolic compounds. Implications of chloride ions. Environ. Sci. Technol. 40, 1000–1007.

Ball, D.L., Edwards, J.O., 1956. The kinetics and mechanism of the decomposition of caros acid.1. J. Am. Chem. Soc. 78, 1125–1129.

Baran, W., Sochacka, J., Wardas, W., 2006. Toxicity and biodegradability of sulfonamides and products of their photocatalytic degradation in aqueous solutions. Chemosphere 65, 1295–1299.

Ben Hammouda, S., Zhao, F., Safaei, Z., Srivastava, V., Ramasamy, D.L., Iftekhar, S., Kalliola, S., Sillanpaa, M., 2017. Degradation and mineralization of phenol in aqueous medium by heterogeneous monopersulfate activation on nano-structured cobalt based-perovskite catalysts ACoO(3) (A = La, Ba, Sr and Ce): characterization, kinetics and mechanism study. Appl. Catal. B Environ. 215, 60–73.

Chan, K.H., Chu, W., 2009. Degradation of atrazine by cobalt-mediated activation of peroxymonosulfate: different cobalt counteranions in homogenous process and cobalt oxide catalysts in photolytic heterogeneous process. Water Res. 43, 2513–2521.

Chen, P., Zhang, Q.X., Su, Y.H., Shen, L.Z., Wang, F.L., Liu, H.J., Liu, Y., Cai, Z.W., Lv, W.Y., Liu, G.G., 2018. Accelerated photocatalytic degradation of diclofenac by a novel CQDs/BiOCOOH hybrid material under visible-light irradiation: dechloridation, detoxicity, and a new superoxide radical model study. Chem. Eng. J. 332, 737–748.

Chen, W., Li, X., Pan, Z., Ma, S., Li, L., 2016. Effective mineralization of Diclofenac by catalytic ozonation using Fe-MCM-41 catalyst. Chem. Eng. J. 304, 594–601.

Corcoran, J., Winter, M.J., Tyler, C.R., 2010. Pharmaceuticals in the aquatic environment: a critical review of the evidence for health effects in fish. Crit. Rev. Toxicol. 40, 287–304.

Delatorre, A., Delgado, B., Lara, C., 1991. Nitrate-dependent O_2 evolution in intact leaves. Plant Physiol. 96, 898–901.

Duan, X.G., Su, C., Miao, J., Zhong, Y.J., Shao, Z.P., Wang, S.B., Sun, H.Q., 2018. Insights into perovskite-catalyzed peroxymonosulfate activation: maneuverable cobalt sites for promoted evolution of sulfate radicals. Appl. Catal. B Environ. 220, 626–634.

EU, 2013. Directive 2013/39/EU of the European parliament and of the council amending directives 2000/60/EC and 2008/105/EC as regards priority substances in the field of water policy. Off. J. Eur. Commun. 226, 1–17.

Flanagan, J., Griffith, W.P., Skapski, A.C., 1984. The active principle of caros acid, HSO_5^--X-ray crystal structure of $KHSO_5H_2O$. J. Chem. Soc., Chem. Commun. 1574–1575.

Gavrilescu, M., Demnerova, K., Aamand, J., Agathoss, S., Fava, F., 2015. Emerging pollutants in the environment: present and future challenges in biomonitoring, ecological risks and bioremediation. N. Biotech. 32, 147–156.

Goodman, J.F., Robson, P., 1963. Decomposition of inorganic peroxyacids in aqueous alkali. J. Chem. Soc. 2871–2875.

Gray, P., 1959. Chemistry of free radicals containing oxygen. 2. Thermochemistry of the hydroxyl and hydroperoxyl radicals. Trans. Faraday Soc. 55, 408–417.

Guan, Y.-H., Ma, J., Li, X.-C., Fang, J.-Y., Chen, L.-W., 2011. Influence of pH on the formation of sulfate and hydroxyl radicals in the UV/peroxymonosulfate system. Environ. Sci. Technol. 45, 9308–9314.

Hao, F., Guo, W., Wang, A., Leng, Y., Li, H., 2014. Intensification of sonochemical degradation of ammonium perfluorooctanoate by persulfate oxidant. Ultrason. Sonochem. 21, 554–558.

Jaafarzadeh, N., Ghanbari, F., Ahmadi, M., 2017. Catalytic degradation of 2,4-dichlorophenoxyacetic acid (2,4-D) by nano-Fe_2O_3 activated peroxymonosulfate: influential factors and mechanism determination. Chemosphere 169, 568–576.

Janzen, E.G., Kotake, Y., Hinton, R.D., 1992. Stabilities of hydroxyl radical spin adducts of PBN-type spin traps. Free Radical Biol. Med. 12, 169–173.

Ji, F., Li, C.L., Wei, X.Y., Yu, J., 2013. Efficient performance of porous Fe_2O_3 in heterogeneous activation of peroxymonosulfate for decolorization of Rhodamine B. Chem. Eng. J. 231, 434–440.

Kolthoff, I.M., Miller, I.K., 1951. The chemistry of persulfate.1. The kinetics and mechanism of the decomposition of the persulfate ion in aqueous medium. J. Am. Chem. Soc. 73, 3055–3059.

Lau, T.K., Chu, W., Graham, N.J.D., 2007. The aqueous degradation of butylated hydroxyanisole by UV/$S_2O_8^{2-}$: study of reaction mechanisms via dimerization and mineralization. Environ. Sci. Technol. 41, 613–619.

Lin, K.-Y.A., Chen, Y.-C., Lin, Y.-F., 2017. $LaMO_3$ perovskites (M=Co, Cu, Fe and Ni) as heterogeneous catalysts for activating peroxymonosulfate in water. Chem. Eng. Sci. 160, 96–105.

Maruthamuthu, P., Neta, P., 1977. Radiolytic chain decomposition of peroxomonophosphoric and peroxomonosulfuric acid. J. Phys. Chem. 81, 937–940.

Miao, J., Sunarso, J., Duan, X.G., Zhou, W., Wang, S.B., Shao, Z.P., 2018. Nano-structured Co-Mn containing perovskites for degradation of pollutants: insight into the activity and stability. J. Hazard Mater. 349, 177–185.

Negri, A.R., Jimenez, G., Hill, R.T., Francis, R.C., 1998. Caroate delignification Part 4: the generation and role of hydroxyl radicals. Tappi J. 81, 241–246.

Neta, P., Huie, R.E., Ross, A.B., 1988. Rate constants for reactions of inorganic radicals in aqueous solution. J. Phys. Chem. Ref. Data 17, 1027–1284.

Olmez-Hanci, T., Arslan-Alaton, I., 2013. Comparison of sulfate and hydroxyl radical based advanced oxidation of phenol. Chem. Eng. J. 224, 10–16.

Olmez-Hanci, T., Arslan-Alaton, I., Dursun, D., 2014. Investigation of the toxicity of common oxidants used in advanced oxidation processes and their quenching agents. J. Hazard Mater. 278, 330–335.

Osman, M.E.H., El-Naggar, A.H., 1999. Role of nitrate in photosynthetic electron transport of Chlorella vulgaris. Photosynthetica 36, 389–395.

Pang, X., Guo, Y., Zhang, Y., Xu, B., Qi, F., 2016. $LaCoO_3$ perovskite oxide activation of peroxymonosulfate for aqueous 2-phenyl-5-sulfobenzimidazole degradation: effect of synthetic method and the reaction mechanism. Chem. Eng. J. 304, 897–907.

Rao, Y., Yang, H., Xue, D., Guo, Y., Qi, F., Ma, J., 2016. Sonolytic and sonophotolytic degradation of Carbamazepine: kinetic and mechanisms. Ultrason. Sonochem. 32, 371–379.

Rao, Y., Zhang, Y., Han, F., Guo, H., Huang, Y., Li, R., Qi, F., Ma, J., 2018. Heterogeneous activation of peroxymonosulfate by $LaFeO_3$ for diclofenac degradation: DFT-assisted mechanistic study and degradation pathways. Chem. Eng. J. 352, 601–611.

Rao, Y.F., Qu, L., Yang, H.S., Chu, W., 2014. Degradation of carbamazepine by Fe(II)-activated persulfate process. J. Hazard Mater. 268, 23–32.

Sein, M.M., Zedda, M., Tuerk, J., Schmidt, T.C., Golloch, A., von Sonntao, C., 2008. Oxidation of diclofenac with ozone in aqueous solution. Environ. Sci. Technol. 42, 6656–6662.

Servin, A.D., Morales, M.I., Castillo-Michel, H., Hemandez-Viezcas, J.A., Munoz, B., Zhao, L., Nunez, J.E., Peralta-Videa, J.R., Gardea-Torresdey, J.L., 2013. Synchrotron verification of TiO_2 accumulation in cucumber fruit: a possible pathway of TiO_2 nanoparticle transfer from soil into the food chain. Environ. Sci. Technol. 47, 11592–11598.

Solis, R.R., Javier Rivas, F., Gimeno, O., 2017. Removal of aqueous metazachlor, tembotrione, tritosulfuron and ethofumesate by heterogeneous monopersulfate decomposition on lanthanum-cobalt perovskites. Appl. Catal. B Environ. 200, 83–92.

Su, C., Duan, X., Miao, J., Zhong, Y., Zhou, W., Wang, S., Shao, Z., 2017. Mixed conducting perovskite materials as superior catalysts for fast aqueous-phase Advanced oxidation: a mechanistic study. ACS Catal. 7, 388–397.

Tan, C.Q., Gao, N.Y., Deng, Y., Deng, J., Zhou, S.Q., Li, J., Xin, X.Y., 2014. Radical induced degradation of acetaminophen with Fe_3O_4 magnetic nanoparticles as heterogeneous activator of peroxymonosulfate. J. Hazard Mater. 276, 452–460.

Wang, Y.R., Chu, W., 2011. Degradation of a xanthene dye by Fe(II)-mediated activation of Oxone process. J. Hazard Mater. 186, 1455–1461.

Wang, Z., Li, J., Zhao, J., Xing, B., 2011. Toxicity and internalization of CuO nanoparticles to prokaryotic alga Microcystis aeruginosa as affected by dissolved organic matter. Environ. Sci. Technol. 45, 6032–6040.

Yang, S., Wang, P., Yang, X., Shan, L., Zhang, W., Shao, X., Niu, R., 2010. Degradation efficiencies of azo dye Acid Orange 7 by the interaction of heat, UV and anions

with common oxidants: persulfate, peroxymonosulfate and hydrogen peroxide. J. Hazard Mater. 179, 552–558.
Yang, Y., Pignatello, J.J., Ma, J., Mitch, W.A., 2014. Comparison of halide impacts on the efficiency of contaminant degradation by sulfate and hydroxyl radical-based advanced oxidation processes (AOPs). Environ. Sci. Technol. 48, 2344–2351.
Zhang, T., Zhu, H., Croue, J.-P., 2013. Production of sulfate radical from peroxymonosulfate induced by a magnetically separable $CuFe_2O_4$ spinel in water: efficiency, stability, and mechanism. Environ. Sci. Technol. 47, 2784–2791.
Zhou, T., Feng, K., Xiang, W., Lv, Y.L., Wu, X.H., Mao, J., He, C., 2018. Rapid decomposition of diclofenac in a magnetic field enhanced zero-valent iron/EDTA Fenton-like system. Chemosphere 193, 968–977.